

Original Research

View Article online



Received 19 February 2025

Revised 12 April 2025

Accepted 12 May 2025

Available Online 03 July 2025

Edited by Prabu Kumar
Seetharaman

KEYWORDS:

Iron sucrose injection
Physicochemical characterization
Ion chromatography
Reduction kinetics
Labile iron
Total iron

Natr Resour Human Health 2025; 5 (3): 438–448
<https://doi.org/10.53365/nrhh/204980>
eISSN: 2583-1194
Copyright © 2025 Visagaa Publishing House

Integrated Quantitative Assessment and Comprehensive Physicochemical Characterization of Pharmaceutical-Grade Intravenous Iron Colloidal Complex: Iron Sucrose

Madhava Krishna Kamisetty¹, Ravada Kishore^{1,*}, Rajesh Medisetty²,
Suresh Penumathsa³, Suresh Pappureddy³, Kashanna Jajula⁴

¹Department of Chemistry, GITAM School of Science, GITAM (Deemed University), Gandhi Nagar, Rushikonda, Visakhapatnam, Andhra Pradesh, India

²Analytical Research and Development, Shilpa Biologicals Pvt. Ltd., Dharwad, Karnataka, India

³Analytical Research and Development, Biological E Limited, Road No. 35, Jubilee Hills, Hyderabad, Telangana, India

⁴Department of chemistry, Indian Institute of Chemical Technology, Rajiv Gandhi University of Knowledge Technologies, Idupulapaya, Vempalli, Kadapa, Andhra Pradesh, India

ABSTRACT: Regulatory approval of iron sucrose similars (ISSs) requires rigorous physicochemical and bioequivalence testing, but their nanoscale colloidal nature complicates characterization. The aim of this study was to evaluate ISSs through quantitative and physicochemical characterization in order to accelerate the development of the ISSs and expedite the launch of its products in the market, ensure its safety, and demonstrate its efficacy of the product. Quantitative assessment included total iron (redox potentiometry/atomic absorption spectrometry [AAS]: 20 mg/mL), carbohydrate content (ion chromatography [IC]: 295–305 mg/mL), labile iron (high-performance liquid chromatography [HPLC]: 0.33–0.61%), and reduction kinetics (T75 as a bio-equivalence marker). Physicochemical characterization was carried out by SEC (Size Exclusion Chromatography), TEM (Transmission Electron Microscopy), XRD (X-ray Diffraction), FT-IR (Fourier Transform Infrared Spectroscopy), UV-Vis (Ultraviolet-Visible Spectroscopy), DLS (Dynamic Light Scattering), and NMR (Nuclear Magnetic Resonance Spectroscopy) as orthogonal techniques to look at the whole particle, iron core, and carbohydrate shell. The results of the study revealed that the particle has an octahedral iron oxyhydroxide core with an akaganeite-like structure, bead diameters of 10.5–11.7 nm, and molecular weights of 41–43 kDa. The NMR was used to confirm the structure of the carbohydrate shell and the FT-IR was used to study the iron core and carbohydrate interactions. These findings demonstrate a comprehensive framework for ISSs evaluation, bridging analytical precision with regulatory requirements for colloidal iron therapeutics.

* Corresponding author.

E-mail address: kravada@gitam.edu (Ravada Kishore)

This is an open access article under the CC BY-NC-ND license (<http://creativecommons.org/licenses/by-nc-nd/4.0/>).

1. INTRODUCTION

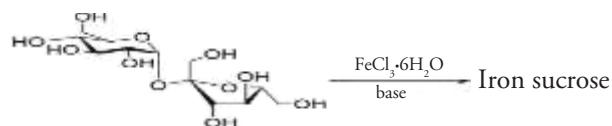
Iron plays a critical role in numerous metabolic processes, including oxygen transport, deoxyribonucleic acid (DNA) synthesis, and energy production; essential for maintaining cardiovascular health, erythrocyte production, immune function, brain development, and cognitive performance; and indispensable for erythropoiesis, enzymatic functions, and mitochondrial energy utilization (Abbaspour et al., 2014; Funk et al., 2022). Iron deficiency, marked by depleted iron stores and iron overload which can lead to cytotoxicity, underscores the necessity of maintaining precise iron homeostasis. Advanced regulatory mechanisms are therefore crucial for balancing iron levels and preventing toxicity. For nearly three centuries, iron has been used to treat anemia, primarily through oral supplementation. While oral iron therapy is cost-effective and widely used, it is often limited by gastrointestinal side effects and the prolonged treatment required to effectively restore iron levels (Silverstein et al., 2004). Early attempts at intravenous iron administration revealed significant risks, particularly with unprotected inorganic ferric iron formulations, such as colloidal ferric hydroxide, which could cause severe adverse effects. These challenges highlighted the need for safer, more advanced iron formulations that ensured controlled release and minimized oxidative stress. To address these concerns, iron-carbohydrate complexes that stabilize colloidal ferric hydroxide particles through carbohydrate chelation were developed, significantly improving the safety of parenteral iron administration (Geisser and Burckhardt, 2011). Intravenous iron complexes are absorbed by macrophages in the reticuloendothelial system (RES), including in the bone marrow, spleen, and liver, enabling efficient iron distribution and utilization (Zou et al., 2017). These complexes consist of a Fe(III) oxyhydroxide core surrounded by a carbohydrate shell composed of polymers such as sucrose, dextran, gluconate, or carboxymaltose, forming spheroidal nanoparticles typically ranging from 8 nm to 30 nm in size (Mühlebach and Flühmann, 2015). The carbohydrate shell prevents aggregation and maintains colloidal stability, ensuring prolonged solubility and bioavailability. Modern intravenous iron formulations are designed to deliver high iron concentrations rapidly while at the same time making sure that it is safe, non-toxic, and stable. The structural arrangement of carbohydrate polymers in iron-carbohydrate complexes is crucial for their functionality, preventing iron colloid aggregation and precipitation. This stability ensures effective delivery and controlled iron release, avoiding rapid release into the bloodstream which could cause toxicity. Unlike the fast-releasing iron formulations that runs the risk of adverse effects or anaphylaxis, iron-carbohydrate complexes balance safety and efficacy. Regulatory agencies like the EU's European Medicines Agency

(EMA) and US Food and Drug Administration (FDA) classify them as nonbiological complex drugs (NBCDs) due to their interdependent structures, where the entire complex acts as the active pharmaceutical ingredient (Danielson, 2004). Functioning as prodrugs, these complexes undergo metabolic transformation to release iron in a regulated manner, aligning with natural iron regulation mechanisms involving transferrin and ferritin. These properties make intravenous iron-carbohydrate complexes a safer, more effective option for treating iron deficiency anemia (IDA).

The physicochemical properties of iron colloids, such as molecular weight (Mp) distribution, particle size, iron colloid stability, and free/labile iron content, significantly impact their safety, efficacy, iron release kinetics, and tissue distribution. Iron core morphology and size influence macrophage uptake and tissue penetration, whereas core stability, iron release, and toxicity depend on factors like iron valence, spin state, coordination, and ligand binding. The carbohydrate shell and its interaction with the iron core further affect colloid stability and biodistribution. Thus, the quality of iron complexes depends on the iron core, carbohydrate shell, and their combined properties, necessitating comprehensive evaluation. Iron sucrose (IS), a widely used iron complex, has numerous global variants with potentially nonequivalent properties. This study focuses on physicochemical techniques to compare IS formulations and establish quality tests for batch release, with findings applicable to other iron-based drugs.

IS contains polynuclear iron(III) hydroxide as an iron core and sucrose as a ligand that covers the inner core of iron to form iron saccharate. The suggested basic formula— $\text{Na}_2\text{Fe}_3\text{O}_8(\text{OH}) \cdot 3(\text{H}_2\text{O}) \cdot n \cdot m(\text{C}_{12}\text{H}_{22}\text{O}_{11})$ —has an average Mw of 34,000–60,000 Da where the number of sucrose molecules associated with iron(III) hydroxide is denoted by “m” and the degree of iron polymerization by “n” (Venofer® [iron sucrose injection]_Labeling).

Preparing an iron-sucrose complex involves reacting ferric chloride with sodium hydroxide to obtain ferric hydroxide, which reacts with sucrose in an aqueous reaction at a selected molar ratio, time, temperature, and pH (potential of hydrogen). The obtained product was isolated as iron(III) hydroxide sucrose, a hygroscopic dark reddish powder easily soluble in water and an active ingredient (Kumar Abvderrcmsprgscvksmas).



General synthetic route representation of iron sucrose.

IS is a sterile, nonpyrogenic solution composed of ferric hydroxide and sucrose dissolved in water for injection. It is a dark, viscous liquid with a pH ranging from 10.5 to 11.0 and an osmolarity between 1150 and 1350 mOsmol/L. To adjust the pH, sodium hydroxide was added. There were no antibacterial agents, chelating agents, dextrans, gluconates, or any other compounds. The solution had a concentration of 20 mg of elemental iron per milliliter of the drug product, roughly equivalent to 30% sucrose w/v (weight in volume) (300 mg/mL) (Monographs USP [Iron Sucrose Injection]). IS quickly dissociates into iron and sucrose via the RES and mostly taken up by transferrin to target cells, including erythroid precursor cells and other proteins, whereas reticuloendothelial macrophages endocytose the iron core (Danielson, 2004; Shah et al., 2014; Venofer® [iron sucrose injection]_Labeling). The iron present in the precursor cells is assimilated into hemoglobin as the cells undergo maturation and transform into red blood cells.

2. MATERIALS AND METHODS

2.1. Materials

Sodium thiosulfate pentahydrate from FINAR; deferoxamine mesylate and iron(III) chloride hexahydrate from Sigma Aldrich; potassium dichromate from Certipur®; hydrochloric acid, calcium chloride, potassium iodide, sodium chloride, tris buffer, methanol, acetonitrile, sodium chloride, and potassium bromide from Merck; 50% NaOH solution (sodium hydroxide solution) from Lobachem; and the Pullulan kit (P-82) from Shodex were procured. The following IV iron preparations with IS were purchased from a pharmacy or directly from the supplier: Orofer® from Emcure, Irorich from Lupin, Biofer-S from Microlabs, and Imax-S from ARISTO from India. Because four lots were utilized, the lot numbers were listed individually for each technique.

2.2. Methods

2.2.1. Total iron determination

Redox iodometry by potentiometric determination with Metrohm Auto titrator instrument (2.095.0010), a validated method, was used to estimate the total iron content (Kamisetty et al. 2023) in the ISSs. This method overcomes the limitations of other techniques such as atomic absorption spectrometry (AAS) (Monographs USP [Iron Dextran Injection]; Monographs USP [Iron Sucrose Injection]; Tabasi et al., 2021), inductively coupled plasma mass spectrometry (ICP-MS) (Brandis et al., 2021; Matta et al., 2018;

Sun et al., 2018), polarography (Barot et al., 2014; Merli et al., 2012), and colorimetric methods (Abbasi et al., 2021; Geisser et al., 1992; Gupta et al., 2016; Qi et al., 2011; Pharmacopoeia B).

2.2.2. Carbohydrate content

Carbohydrate content was determined on the ISSs using ion chromatography (IC) with optimized conditions. A 10 µL sample was separated on a Carbowax PA1 column (4 mm × 250 mm) and guard column (4 mm × 50 mm) with a 100 mM NaOH mobile phase in a 15-minute run. The Thermo Scientific Dionex ICS 5000+ system, equipped with Chromeleon software 7, was used with high-performance anion exchange chromatography and pulsed amperometric detection. The flow rate was 1 mL/minute with the detector, column, and autosampler set at 30°C, 25°C, and 25°C, respectively. Standard sucrose and sample solutions were analyzed using a gold working electrode and an Ag/AgCl (silver/silver chloride) reference electrode.

2.2.3. Dynamic light scattering

Diluted ISS hydrodynamic diameters were measured using a Zetasizer ZSP (Malvern Instruments, Worcestershire, UK) and analyzed with Zetasizer software 7.11 (Brandis et al., 2021). Measurements were based on Brownian motion and performed in a single-use cuvette. Backscattering data were collected at 173° using a 633 nm He-Ne laser. Refractive index and viscosity were set to 1.330 and 0.8872 cP (centipoise), respectively. The optimum position was determined with a 120-second equilibration time at 25.0°C. Results were averaged from three subruns each with ≥ 12 measurements and interpreted using intensity-based Z-average. System suitability was verified before each experiment using a 60 nm (± 3 nm) polystyrene nanosphere standard.

2.2.4. Size exclusion chromatography

The Mp of ISSs complexes were analyzed using size exclusion chromatography (SEC) adapted from the USP (United States pharmacopeia) IS monograph with modifications. Samples (25 µL) were separated on two Shodex columns (300 × 7.8 mm, 13 µm particle size) composed of hydrophilic polyhydroxymethacrylate gel particles connected in series. A pullulan polysaccharide standard kit (5000–800,000 Da) was used for calibration. Standards (1 mg/mL) and samples (5 mg/mL) were prepared in ultrapure water. The analysis was performed on a Waters Alliance HPLC (high-performance liquid chromatography) system with a refractive index detector, column, and autosampler set at 45°C, 45°C and 25°C, respectively, using Empower 3.6.1.1 software at a flow rate of 0.5 mL/minute. A calibration curve was constructed by plotting retention times against peak top Mp with a correlation

coefficient ≥ 0.98 . Mp of ISS complexes were determined by comparing their retention times to the calibration curve.

2.2.5. Reduction kinetics

Kinetic analysis of the reduction method was proposed by Shah (Mandal SSPDDKSVPK, 2018). The ISSs were analyzed by colorimetric determination using a SpectraMax[®] i3x Multi-Mode Microplate reader (Molecular Devices, Silicon Valley, CA, USA) at 450 nm with SoftMax Pro7.0.3 GxP. The kinetics of IS were measured for 80 minutes and the data points were collected at intervals of 5 minutes. The adopted method met the following criteria: a T_{75} reduction time. The reduction kinetics data points were plotted for “log (percentage of trivalent iron concentration) versus time” (Mandal SSPDDKSVPK, 2010; Mary Jane Helenek RAL, 2013).

2.2.6. Chelatable iron determination

The validated analytical method was adopted from Tesoro et al. (2005) and Pai et al. (2017, 2018). The chromatographic conditions were modified to improve the resolution of the intact complex with the chelated iron-deferoxamine (Fe-DFO) complex, feroxamine (FO), and the DFO. Each 20 μ L sample was subjected to chromatographic separation using a C8 column composed of dimethyl-n-octyl silane with Rx-SIL (small diameter porous silica particle) bonding, 150 mm \times 4.6 mm dimensions and a 3.5 μ m particle size. The experiment was conducted with solvent A (Tris-HCl [tris(hydroxymethyl)aminomethane hydrochloride]) and solvent B (methanol) as the mobile phase using a gradient of 0–10 minutes (75% A), 15–20 minutes (25% A), and 21–30 minutes (75% A) at a 0.5 mL/minute flow rate on a Waters Alliance HPLC system with a photodiode array detector set at 430 nm and column and autosampler set at 30°C and 25°C with a run time of 30 minutes using Empower 3.6.1.1 software.

2.2.7. X-ray diffraction

X-ray diffraction (XRD) measurements were conducted on ISSs using a Bruker D8 Advance powder X-ray diffractometer with Cu K α (copper K-alpha) radiation (1.54060 Å [Angstrom]) and a LYNXEYE XE-T detector. Liquid samples were dried for three hours to prevent breakage of the material. The diffractometer was calibrated using a corundum standard sample and data analysis was performed using DIFFRAC.EVA Version 4.3.1.2 and the Bruker TOPAS software. The parameters for the slow-scan measurements were primary soller slit 2.5°; air scatter automatic, divergence slit 0.3°; anti-scatter slit 8 mm; secondary soller slit 2.5°; 2 θ range 5–90°; step size 0.03°; time/step 2.5 seconds; and measurement time 2 hours. The GOF (goodness of fit) parameter was used to assess the pact between the model and data, with a GOF of 1.0 indicating a perfect fit.

2.2.8. Transmission electron microscopy

ISSs complex nanoparticle size and morphology were examined at ambient temperature using a JEOL JEM F200 transmission electron microscope. Diluted samples of Milli-Q water were dried with nitrogen using a Lacey C Film 400 copper mesh grid. Electron micrographs were captured with bright and dark fields at the exact locations where SAED (Selected Area Electron Diffraction) patterns were recorded. The samples were analyzed using the EMSIS software where the geometrical mean particle diameter (dg) was determined.

2.2.9. UV-visible absorption spectroscopy

ISS samples absorbance was measured in the range of 800–200 nm wavelength to collect spectral data. The absorption spectra were measured using a Perkin-Elmer Lambda 800 UV/VIS spectrophotometer with UV Win Lab 3.00.03. Milli-Q water was used as a blank and the path length was measured to be 1 cm. The molar extinction coefficients were calculated by measuring the absorbance at wavelengths of 300 nm and 470 nm, considering the molar quantity of iron in each sample.

2.2.10. Fourier transform infrared spectroscopy

The ISS injection sample was freeze-dried using a freeze-dry lyophilizer (Labconco, Model: Triad). An established iron-leaching process was used in both IS formulations to remove iron, and the corresponding iron-free liquid supernatants (carbohydrate syrups) were further freeze-dried. A homogenous fine mixture was obtained by pulverizing 3 mg of freeze-dried IS samples and iron-leached sucrose at a ratio of 1:100 with 300 mg of potassium bromide (KBr). The mixture was pelleted using a mechanical press, subjected to infrared analysis using an FTIR spectrometer (Shimadzu, Kyoto, Japan) and analyzed using the IR Affinity-1 software where 45 accumulations were counted. The 4000–400^{cm}⁻¹ range was used for sample scanning with a resolution of 4^{cm}⁻¹. As a blank, KBr FT-IR spectrum was also obtained.

2.2.11. Nuclear magnetic resonance spectroscopy

The ISSs sample was dissolved in deuterium oxide (D₂O) with 0.05 weight percentage 3-(trimethylsilyl)-2,2,3,3-tetra-deuteriopropionic acid (TSP-d₄) and transferred to a 5 mm NMR (Nuclear Magnetic Resonance Spectroscopy) tube. NMR spectra were acquired for protons and carbon at 27°C using a JEOL (600 MHz) NMR spectrometer (Model: ECZR) with delta-processing software version 5.3.3. ¹³C spectra for the IS sample were acquired as such. For ¹H spectra, IS samples were processed by leaching iron where sucrose alone was analyzed (used from the FT-IR).

3. RESULTS AND DISCUSSION

3.1. Total iron determination

The average iron content measured using redox potentiometry and AAS ranged from 20 mg/mL to 21 mg/mL (Labeled claim of IS 20 mg/mL). Details are presented in Table 1. IS products, such as Iroch (20 ± 0.1 mg/mL) and Biofer-S (20 ± 0.3 mg/mL), align closely with the labeled claim of 20 mg/mL. However, minor deviations were observed in Orofer® (21 ± 0.3 mg/mL) and Imax-S (21 ± 0.3 mg/mL), which are within acceptable limits (± 5%). The low standard deviations (from ± 0.1 to ± 0.3 mg/mL) across batches highlight the robustness of the analytical method used. These results show that the results obtained from redox potentiometry and AAS methodologies for ISSs are acceptable according to the predetermined criteria outlined in the IS monograph of the USP (Brasted, 1952; Swift, 1929). Therefore, the redox potentiometry results were similar to those of advanced techniques, such as AAS. Hence, the use of redox potentiometry to quantify total iron is a reliable technique that can be implemented in quality control laboratories (Kamisetty et al., 2023).

3.2. Carbohydrate content

The carbohydrate content determined using IC for the ISSs ranged from 295 mg/mL to 305 mg/mL. Chromatographic details and results are provided in Figure 1A and Table 1, respectively. These results meet the USP's proposed batch release acceptability limit for IS (260–340 mg/mL) (Funk, 2022; Monographs USP [Iron Sucrose Injection]). Based on these findings, IS requires 15 times more saccharides than iron. The carbohydrate assay results were previously determined using anthrone reagent with a spectrophotometer (Geisser et al., 1992) and an HPLC system with a refractive index detector (Monographs USP [Iron Sucrose Injection]). Colorimetric techniques are more variable and less sensitive. Refractive index detectors are less sensitive, interfere with temperature and pressure fluctuations, and require a longer detector stabilization time. For a more advanced approach, chromatography can be utilized because it has better matrix tolerance and is more sensitive. The determination of carbohydrates by anthrone for the IS drug product was 318–392 mg/mL in three lots (Funk et al., 2022). The results obtained using the current IC method align with the reported values for IS (Geisser et al., 1992).

3.3. Dynamic light scattering

ISSs size was determined using dynamic light scattering (DLS). The Z-average values of the ISSs ranged from

10.5 nm to 11.7 nm (Table 2). The results were in accordance with the previously reported Z-average sizes of 11.4 nm (Wu et al., 2016), 11.6nm, 12.2nm, 12.4nm (Di Francesco and Borchard, 2018), 10.1 nm (Shah et al., 2014; Zou et al., 2017), 11.9 nm (Using DLS, ELS and SAXS to Study Ferric Nanoparticles), and 10.1 nm (Di Francesco et al., 2017; Venofer® [iron sucrose injection]_Labeling). The FDA recommends DLS as a critical in vitro study for evaluating colloidal iron drugs due to its ability to provide precise data on particle size and size distribution. DLS is particularly effective for analyzing smaller, homogeneously distributed particles (Barot et al., 2014). The polydispersity index (PDI) is a key parameter for quantifying particle size variability, with values ranging from 0 to 1. A PDI < 0.1 indicates monodisperse particles, while values > 0.1 suggest polydisperse distributions. For ISSs, a polydisperse distribution was observed with a primary size of 11 d.nm and a PDI of 0.21 (Di Francesco and Borchard, 2018). The results are provided in Table 2, and the second peak detected by the instrument in the IS may be a carbohydrate contamination with a lower percentage (Di Francesco and Borchard, 2018). A diagram of the IS sample size distribution is shown in Figure 1B.

3.4. Size exclusion chromatography

The Mw of ISSs were determined using SEC-HPLC, ranging from 41 kDa to 43 kDa (Table 2). Mp is critical for the safety and efficacy of iron-sucrose formulations, as it influences pharmacodynamic properties (Barot et al., 2014). Chromatographic retention times reflected ferric oxyhydroxide polymerization (Shah et al., 2014) and showed a homogeneous distribution (Barot et al., 2014). Key parameters (Mw [weight average molecular weight], Mn [number average molecular weight], Mw/Mn) in Table 2 confirmed compliance with IS specifications, validating the method's effectiveness. Chromatograms revealed two peaks post-solvent: a larger peak (sucrose and chloride) and a smaller peak (carbonate and hydroxide mixture) (Neiser et al., 2015). The initial high molecular weight fraction corresponded to iron-carbohydrate nanoparticles (Figure 1C). Although Mp are not absolute, they did enable relative comparisons of hydrodynamic volumes (Inventors Zhang et al., 2021).

3.5. Reduction kinetics

UV/Vis spectrophotometry is a quick technique for determining the bioequivalence of iron reduction kinetics of iron (III) to iron (II) in the ISSs. The rate at which ascorbic acid converts iron (III) to iron (II) according to the kinetics was

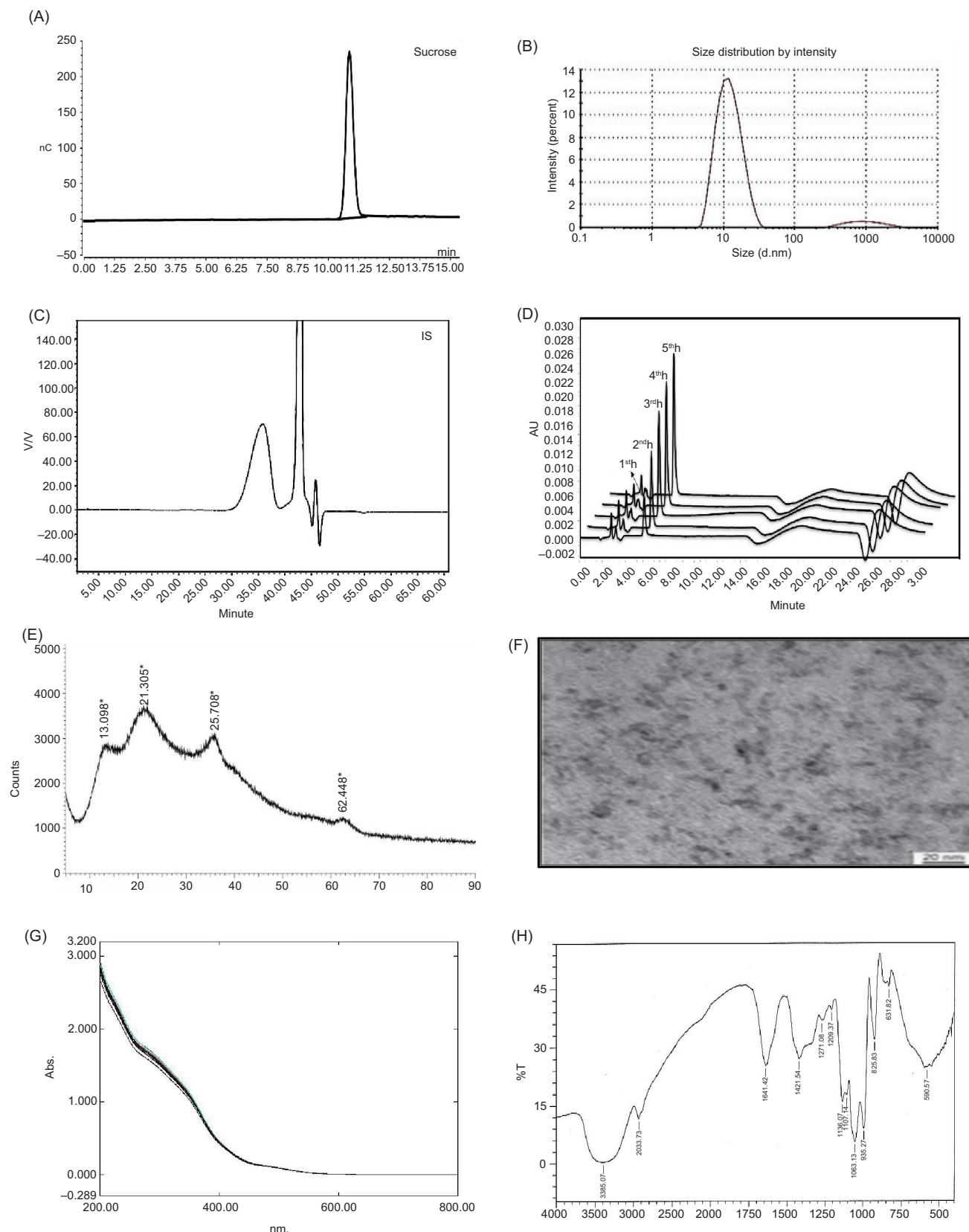


Figure 1. (A) Typical chromatogram of iron sucrose (B) Distribution of size by intensity for IS (C) SEC chromatogram of IS (D) Representative chromatogram showing the release of labile iron from IS (E) PXRD pattern of IS (F) TEM image of the IS (G) Absorption spectra of overlaid ISS (H) FT-IR spectra of IS.

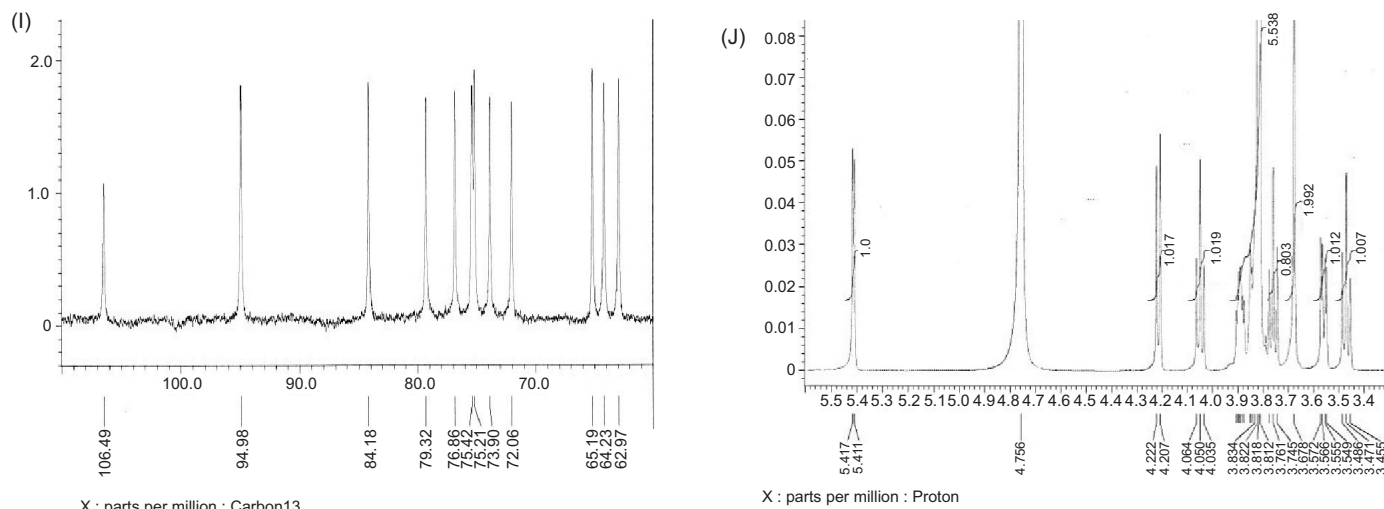


Figure 1. (Continued). (I) ^{13}C spectrum of IS (J) ^1H spectrum of iron-leached sucrose.

Table 1

Results of total iron and carbohydrate content.

Lot No.	Mean value by Potentiometry (mg/mL) (n=3) [§]	Accuracy of labeled amount (%) (n=3) [§]	Mean value by AAS (mg/mL) (n=3) [§]	Accuracy of labeled amount (%) (n=3) [§]	Carbohydrate content (mg/mL) (n=3) [§]
ELF8BK0006	21 ± 0.3	104 ± 1.5	20 ± 0.2	101 ± 0.8	302 ± 5.2
C2WBK07	20 ± 0.1	101 ± 0.7	20 ± 0.1	102 ± 0.6	305 ± 3.1
BISA006	20 ± 0.3	102 ± 1.6	21 ± 0.4	103 ± 2.2	295 ± 6.0
MPA230154	21 ± 0.3	103 ± 1.4	20 ± 0.1	103 ± 0.5	299 ± 3.3

§ = The data presented as the mean plus or minus the standard deviation (mean ± SD).

Table 2

SEC-HPLC and DLS data.

Lot No.	SEC-HPLC determination of weight average molecular weights			Z-average dynamic light scattering and PDI	
	Mw (kDa) (n=3) [§]	Mn (kDa) (n=3) [§]	PDI (n=3) [§]	Z-Average diameter (n=3) [§]	PDI (n=3) [§]
ELF8BK0006	43 ± 0.1	32 ± 0.2	1.38 ± 0.01	11.7 ± 0.1	0.21 ± 0.02
C2WBK07	42 ± 0.2	32 ± 0.6	1.36 ± 0.02	10.7 ± 0.1	0.23 ± 0.01
BISA006	43 ± 0.2	32 ± 0.2	1.37 ± 0.02	10.5 ± 0.3	0.22 ± 0.01
MPA230154	41 ± 0.1	31 ± 0.1	1.33 ± 0.02	11.4 ± 0.2	0.27 ± 0.04

§ = The data presented as the mean plus or minus the standard deviation (mean ± SD).

determined. The T_{75} values obtained for all ISSs of 23.9 ± 0.3 minutes with a correlation greater than 0.98 agree with the previously reported data. Assessing iron supplement bioequivalence requires comprehensive physicochemical characterization beyond iron kinetics. Key parameters include iron core properties (crystalline structure, environment, size), particle morphology, carbohydrate shell composition, surface characteristics, and labile iron detection.

3.6. Chelatable iron determination

Paffetti and Nilsson defined “free” iron as low molecular weight iron not bound by high-affinity plasma proteins or biomolecules in bodily fluids, representing the fraction dissolvable without reductive or complex agents. Labile iron, bound to the iron-carbohydrate matrix, circulates in the blood and resists dialysis. Plasma proteins and chelation agents can

increase dialyzable iron by mobilizing labile iron. Chelation assays cannot distinguish free from labile iron, making “chelatable iron” a more accurate term. The amounts of chelatable iron (free and labile iron) obtained from the ISSs were in the range from 0.33% to 0.61% under in vitro conditions. A earlier study reported that 3.8% of iron was chelatable via EDTA (ethylenediaminetetraacetic acid) chelation (Zou et al., 2018), and this study used DFO chelation. Different chelators yield varying absolute quantities but similar profiles. Labile iron comparisons between iron colloid products under identical conditions of their iron release kinetics are shown in Figure 1D.

3.7. X-ray diffraction

XRD analysis revealed distinct patterns for iron oxyhydroxide and iron oxide crystallites in IS. The IS diffractogram exhibited peaks at 13.0°, 21.3°, 35.7°, and 62.4°, with 13.0° and 21.3° attributed to amorphous sucrose, potentially masking iron-carbohydrate cores (Barot et al., 2014; Barot et al., 2014; Gutiérrez et al., 2005; Kudasheva et al., 2004; Zou et al., 2018). The peak at 35.7° indicated iron oxides, aligning with akageneite-like structures, whereas the 62.4° peak suggested Cl⁻ anions (Barot et al., 2014; Barot et al., 2014; Jahnet al., 2011; Kudasheva et al., 2004), consistent with akageneite's tunnel structure. Supported by SAED data, comparisons with ferrihydrite patterns at 2θ values of 36° and 62° indicated a shift of iron ions toward oxygen planes. Previous studies identified IS as a mix of goethite-akageneite, ferrihydrite, lepidocrocite, or akageneite, with recent findings highlighting ferroxhyte (δ-FeOOH) as the major phase. Reported crystallite sizes ranged from 1 nm to 5 nm, with this study confirming an iron core diameter of 3.3 nm (Figure 1E). Due to IS cores' low crystallinity and small size, XRD alone is insufficient, necessitating complementary techniques like TEM, and Mössbauer spectroscopy for comprehensive characterization.

3.8. Transmission electron microscopy

Bead-like structures were observed in the IS TEM image in Figure 1F. The core size distribution for IS was 1.0–6.0 nm, and the average size of the iron core determined in this study was 3.6 ± 2.2 nm ($n = 20$). These data are similar to the previously reported data of 3 ± 2 nm (Balakrishnan et al., 2009; Kudasheva et al., 2004), 2.92 ± 0.01 nm, 2.77 ± 0.63 nm (Barot et al., 2014). These differences in size may be due to inconsistencies in the concentration of samples, preparation, instruments, parameters, and data processing. Additional evaluations using appropriate methods are required.

3.9. UV-visible absorption spectroscopy

The molar extinction coefficients for IS were determined at 300 nm (from 3132.9 ± 6.45 to 3215.4 ± 4.68 M⁻¹ cm⁻¹) and 470 nm (from 378.6 ± 0.21 to 401.7 ± 0.75 M⁻¹ cm⁻¹), corresponding to oxymetal charge transfer and d-d (d-orbital to d-orbital) transitions, respectively (Barot et al., 2014; Kudasheva et al., 2004). The spectra are characteristic of high-spin Fe (III) complexes with octahedral geometry and a d⁵ configuration. The 300/470 nm extinction coefficient ratio of ~8 aligns with the reported values for IS, confirming the presence of a ferric oxyhydroxide core (Koralewski et al., 2013). These results, consistent with the literature (2600–3000 M⁻¹ cm⁻¹ at 300 nm and 300–400 M⁻¹ cm⁻¹ at 470 nm), validate the structural and electronic properties of the complex (the corresponding data are provided in Table 3 and the spectra in Figure 1G).

3.10. Fourier transform infrared spectroscopy

The structure of the carbohydrate shell and iron core interactions in iron formulations were analyzed using the Fourier transform infrared spectroscopy (FT-IR), a technique effective

Table 3

Results of the IS average absorbance spectra molar extinction coefficients.

Lot no.	Labeled claim (mg/mL)	Fe Conc. (mg/mL)	Cell path length (cm)	ϵ_{300} (M ⁻¹ cm ⁻¹) (n=3) [§]	ϵ_{470} (M ⁻¹ cm ⁻¹) (n=3) [§]	$\epsilon_{300}/\epsilon_{470}$ [#] (n=3) [§]
ELF8BK0006	20	0.03	1	3132.9 ± 6.45	393.3 ± 0.47	8 ± 0.02
C2WBK07	20	0.03	1	3215.4 ± 4.68	401.7 ± 0.75	8 ± 0.22
BISA006	20	0.03	1	3110.6 ± 4.93	378.6 ± 0.21	8 ± 0.41
MPA230154	20	0.03	1	3168.3 ± 6.45	380.6 ± 0.47	8 ± 0.07

§ = The data presented as the mean plus or minus the standard deviation (mean \pm SD) and # rounded values.

in distinguishing oxidized from nonoxidized substances. Group frequencies (above 1500 cm^{-1}) and fingerprint bands (below 1500 cm^{-1}) provide distinct absorption patterns for characterizing polysaccharides. FT-IR spectra of IS revealed significant differences from pure sucrose, indicating complex formation (Figure 1H). Key peaks included 3385 cm^{-1} (OH [hydroxyl] groups), 2933 cm^{-1} (intermolecular hydrogen bonds), 2890 cm^{-1} (C-H [carbon-hydrogen] stretching), and $1400\text{--}1000\text{ cm}^{-1}$ (C-O [carbon-oxygen] stretching). Owing to the Fe-O vibrations, the compound displays six bending vibrations of water molecules at 1641 cm^{-1} and bands in the 580 cm^{-1} region, with the bands matching those previously reported by Venofer (Venofer® [iron sucrose injection]_Labeling). FT-IR spectra of iron-carbohydrate formulations such as IS and iron dextran were analyzed under identical conditions. The overlay spectra showed similar profiles with minor differences in peak shape and intensity within the $1500\text{--}500\text{ cm}^{-1}$ fingerprint region. The purity index between IS and iron dextran was 0.6589, confirming FT-IR's ability to differentiate iron-carbohydrate complexes, as their correlation was below 0.99. The complexity of polysaccharide characterization via FT-IR is due to the structural similarities and band overlap, requiring analysis of multiple spectral regions ($4000\text{--}2500\text{ cm}^{-1}$, $1800\text{--}1500\text{ cm}^{-1}$, $1500\text{--}1200\text{ cm}^{-1}$, $1200\text{--}800\text{ cm}^{-1}$, and below 800 cm^{-1}) for accurate interpretation.

3.11. Nuclear magnetic resonance spectroscopy

Functional groups can be used to classify carbohydrates as stabilizers in ferric preparations. Sucrose-containing preparations may serve as ligands or interact with the ferric (hydr)oxide particles. Iron (III)-containing preparations' ^{13}C NMR signals were cancelled out by the paramagnetic center's binding, and only the nonmetal-bonded molecules were detected by the Evans effect in NMR spectroscopy. Along with being down-field-shifted and widened, the signals are also affected by the

iron content (Kästele et al., 2014). The chemical shifts obtained from ^{13}C NMR of IS are C1-94.98, C2-73.90, C3-75.42, C4-72.06, C5-75.21, C6-62.97, C7-64.23, C8-106.49, C9-79.32, C10-76.86, C11-84.18, and C12-65.19; ^1H NMR was attributed to H1-5.41(d), H2-3.55(dd), H3-3.75(t), H4-3.45(t), H5-3.82(m), H6-3.81(m), H7-3.67(m), H9-4.20(d), H10-4.03(t), H11-3.83(m), and H12-3.81(m), which suggested iron molecule complexation and matched with the previously reported chemical shifts (Barot et al., 2014; Inventors Zhang et al., 2021) (Figure 1I and 1J). Carbon signals expand in the presence of iron, whereas proton signals do not (Barot et al., 2014; Inventors Zhang et al., 2021). The structure of the IS is shown in Figure 2.

4. CONCLUSION

Multiple analytical techniques were employed to characterize ISS complexes, examining their complete structure (iron core + carbohydrate shell) as well as individual components quantitatively. The measured iron and carbohydrate contents matched label claims, with method validation confirming accuracy. DLS measurements of particle size, Mw, and T_{75} values correlated well with the published data, though minor batch-to-batch variations in chelatable iron content were observed. UV-Vis and TEM analysis confirmed consistent ferric octahedral coordination and core morphology across samples. XRD analysis revealed crystallinity uncertainties due to data limitations, with phase identifications that included various iron oxyhydroxides. Complementary TEM-XRD proved valuable for analyzing low-crystallinity nanomaterials. FT-IR and NMR spectroscopy elucidated carbohydrate-specific interactions with the iron core, verifying a sucrose-stabilized polynuclear Fe (III) oxyhydroxide structure in all ISS formulations. These comprehensive characterizations revealed how variations in nanoparticle properties (size, morphology, core-shell interactions) influence therapeutic performance.

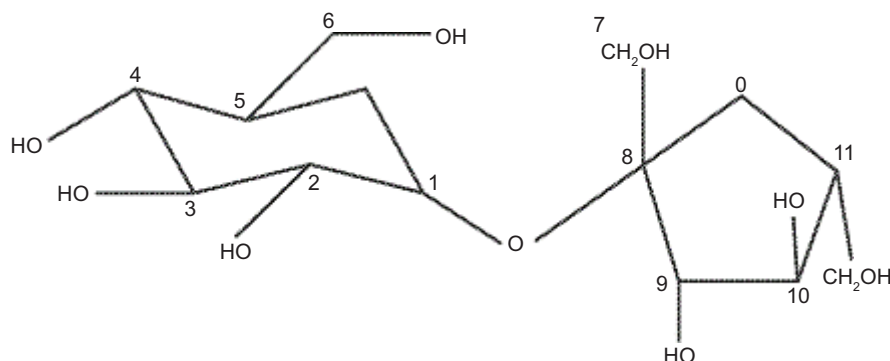


Figure 2. Representative structure of iron sucrose.

Characterization of iron colloids is a complicated and variable process that requires many approaches to obtain accurate and reliable information. A head-to-head comparison study helps minimize variations in the methods; however, it is important to note that the quality of the data and conclusions can be influenced by factors such as sample preparation, experimental settings, and data interpretation. Both the proposed qualitative characterization and quality-impacting quantitative methodology approaches have the potential to be appropriate for evaluating colloidal iron medicines.

ACKNOWLEDGMENTS

The authors express their gratitude to GITAM (Deemed to be University) for providing support for the research activity and Biological E. Limited for data analysis.

AUTHOR CONTRIBUTIONS

Research concept and design: K.R., M.K.K.; Collection and/or assembly of data: S.P., K.J.; Data analysis and interpretation: M.K.K.; Writing the article: S.P.; Critical revision of the article, K.R., R.M.; Final approval of the article, K.R.. All authors have read and agreed to the published version of the manuscript.

CONFLICTS OF INTEREST

There are no conflicts to declare, financial or otherwise.

ORCID

Kishore Ravada	0000-0002-7570-8447
Madhava Krishna Kamisetty	0000-0001-6986-1384
Rajesh Medisetty	0009-0003-8635-8854
Suresh Penumathsa	0000-0002-9961-4349
Suresh Pappureddy	0009-0006-9285-7678
Kashanna Jajula	0000-0002-7248-170X

REFERENCES

- Abbaspour, N., Hurrell, R., Kelishadi, R., 2014. Review on iron and its importance for human health. *Journal of Research in Medical Sciences*. 19(2), 164–174.
- Abbasi, U., Abbina, S., Gill, A., Bhagat, V., Kizhakkedathu, J.N., 2021. A facile colorimetric method for the quantification of labile iron pool and total iron in cells and tissue specimens. *Scientific Reports*. 11(1), 6008. <https://doi.org/10.1038/s41598-021-85387-z>
- Balakrishnan, V.S., Rao, M., Kausz, A.T., Brenner, L., Pereira, B.J., Frigo, T.B., Lewis, J.M., 2009. Physicochemical properties of ferumoxytol, a new intravenous iron preparation. *European Journal of Clinical Investigation*. 39(6), 489–496. <https://doi.org/10.1111/j.1365-2362.2009.02130.x>
- Barot, B.S., Parejiya, P.B., Mehta, D.M., Shelat, P.K., Shah, G.B., 2014. Physicochemical and structural characterization of iron-sucrose formulations: A comparative study. *Pharmaceutical Development and Technology*. 19(5), 513–520. <https://doi.org/10.3109/10837450.2013.795171>
- Barot, B., Parejiya, P., Shelat, P., Shah, G., Mehta, D., Pathak, T., 2014. Physicochemical and toxicological characterization of sucrose-bound polynuclear iron oxyhydroxide formulations. *Journal of Pharmaceutical Investigation*. 45. <https://doi.org/10.1007/s40005-014-0143-2>
- Brandis, J.E.P., Kihn, K.C., Taraban, M.B., Schnorr, J., Confer, A.M., Batelu, S., Sun, D., Rodriguez, J.D., Jiang, W., Goldberg, D.P., 2021. Evaluation of the physicochemical properties of the iron nanoparticle drug products: Brand and generic sodium ferric gluconate. *Molecular Pharmaceutics*. 18(4), 1544–1557. <https://doi.org/10.1021/acs.molpharmaceut.0c00922>
- Brasted, R.C., 1952. Iodometric codetermination of copper and iron. *Analytical Chemistry*. 24(6), 1040–1041. <https://doi.org/10.1021/ac60066a042>
- Danielson, B.G., 2004. Structure, chemistry, and pharmacokinetics of intravenous iron agents. *Journal of the American Society of Nephrology*. 15(Suppl 2), S93–S98.
- Di Francesco, T., Borchard, G., 2018. A robust and easily reproducible protocol for the determination of size and size distribution of iron sucrose using dynamic light scattering. *Journal of Pharmaceutical and Biomedical Analysis*. 152, 89–93. <https://doi.org/10.1016/j.jpba.2018.01.029>
- Di Francesco, T., Philipp, E., Borchard, G., 2017. Iron sucrose: Assessing the similarity between the originator drug and its intended copies. *Annals of the New York Academy of Sciences*. 1407(1), 63–74. <https://doi.org/10.1111/nyas.13517>
- Funk, F., Flühmann, B., Barton, A.E., 2022. Criticality of surface characteristics of intravenous iron-carbohydrate nanoparticle complexes: Implications for pharmacokinetics and pharmacodynamics. *International Journal of Molecular Sciences*. 23(4). <https://doi.org/10.3390/ijms23042140>
- Geisser, P., Baer, M., Schaub, E., 1992. Structure/histotoxicity relationship of parenteral iron preparations. *Arzneimittel-Forschung*. 42(12), 1439–1452.
- Geisser, P., Burckhardt, S., 2011. The pharmacokinetics and pharmacodynamics of iron preparations. *Pharmaceutics*. 3(1), 12–33. <https://doi.org/10.3390/pharmaceutics3010012>
- Gupta, A., Pratt, R.D., Crumbliss, A.L., 2016. Ferrous iron content of intravenous iron formulations. *BioMetals*. 29(3), 411–415. <https://doi.org/10.1007/s10534-016-9923-7>
- Gutiérrez, L., del Puerto Morales, M., José Lázaro, F., 2005. Magnetostructural study of iron sucrose. *Journal of Magnetism and Magnetic Materials*. 293(1), 69–74. <https://doi.org/10.1016/j.jmmm.2005.01.045>
- Inventors Zhang, J., Yongfeng, Luo, Mary, Zi-ping, Ding, Jie, Fei, Wei, Justin, Jun, Bao, Rihard; NMR Methods for Characterizing Iron Sucrose. World Intellectual Property Organization. 2021.

- Jahn, M.R., Andreassen, H.B., Fütterer, S., Nawroth, T., Schünemann, V., Kolb, U., Hofmeister, W., Muñoz, M., Bock, K., Meldal, M., Langguth, P., 2011. A comparative study of the physicochemical properties of iron isomaltoside 1000 (Monofer), a new intravenous iron preparation and its clinical implications. *European Journal of Pharmaceutics and Biopharmaceutics*. 78(3), 480–491. <https://doi.org/10.1016/j.ejpb.2011.03.016>
- Kamisetty, M.K., Medisetty, R., Ramesh, B., Pappureddy, S., Kashanna, J., Govinda, V., Kishore, R., 2023. An analytical method for determination of total iron in pharmaceutical grade intravenous iron colloidal complexes by redox-potentiometry. *Pharmaceutical Nanotechnology*. 11(5) 486–492. <https://doi.org/10.2174/2211738511666230507190224>
- Kästele, X., Sturm, C., Klüfers, P., 2014. C NMR spectroscopy as a tool for the in situ characterisation of iron-supplementing preparations. *European Journal of Pharmaceutics and Biopharmaceutics*. 86(3), 469–477. <https://doi.org/10.1016/j.ejpb.2013.11.003>
- Koralewski, M., Pochylski, M., Gierszewski, J., 2013. Magnetic properties of ferritin and akaganeite nanoparticles in aqueous suspension. *Journal of Nanoparticle Research*. 15(9), 1902. <https://doi.org/10.1007/s11051-013-1902-0>
- Kudasheva, D.S., Lai, J., Ulman, A., Cowman, M.K., 2004. Structure of carbohydrate-bound polynuclear iron oxyhydroxide nanoparticles in parenteral formulations. *Journal of Inorganic Biochemistry*. 98(11), 1757–1769. <https://doi.org/10.1016/j.jinorgbio.2004.06.010>
- Kumar Abvderrcmsprgcsvksmas. Process for preparation of iron sucrose. United States Patent application Publication. 2015.
- Mandal SSPDDKSVPK. In-vitro method for testing bioequivalence of iron-sucrose formulation. Worldwide applications. 2010.
- Mary Jane Helenek RAL, Richard P. Lawrence. Methods and compositions for administration of iron. United States Patent. 2013.
- Matta, M.K., Beekman, C.R., Gandhi, A., Narayanasamy, S., Thomas, C.D., Mohammad, A., Stewart, S., Xu, L., Chockalingam, A., Shea, K., Patel, V., Rouse, R., 2018. Determination of non-transferrin bound iron, transferrin bound iron, drug bound iron and total iron in serum in a rat after IV administration of sodium ferric gluconate complex by simple ultrafiltration inductively coupled plasma mass spectrometric detection. *Nanomaterials*. 8(2). <https://doi.org/10.3390/nano8020101>
- Merli, D., Profumo, A., Dossi, C., 2012. An analytical method for Fe(II) and Fe(III) determination in pharmaceutical grade iron sucrose complex and sodium ferric gluconate complex. *Journal of Pharmaceutical Analysis*. 2(6), 450–453. <https://doi.org/10.1016/j.jpha.2012.05.003>
- Monographs USP FDA. USP Monographs, Iron Dextran Injection USP-NF.
- Monographs USP FDA. USP Monographs, Iron Sucrose Injection USP-NF.
- Mühlebach, S., Flühmann, B., 2015. Iron Carbohydrate Complexes: Characteristics and Regulatory Challenges. Springer International Publishing, Switzerland, 149–170 pp. https://doi.org/10.1007/978-3-319-16241-6_5
- Neiser, S., Rentsch, D., Dippon, U., Kappler, A., Weidler, P.G., Göttlicher, J., Steiningere, R., Wilhelma, M., Braitscha, M., Funka, F., Philippa, E., Burckhardt, S., 2015. Physico-chemical properties of the new generation IV iron preparations ferumoxytol, iron isomaltoside 1000 and ferric carboxymaltose. *BioMetals*. 28(4), 615–635. <https://doi.org/10.1007/s10534-015-9845-9>
- Pai, A.B., Meyer, D.E., Bales, B.C., Cotero, V.E., Pai, M.P., Zheng, N., Jiang, W., 2017. Performance of redox active and chelatable iron assays to determine labile iron release from intravenous iron formulations. *Clinical and Translational Science*. 10(3), 194–200. <https://doi.org/10.1111/cts.12443>
- Pai, A.B., Pai, M.P., Meyer, D.E., Bales, B.C., Cotero, V.E., Zheng, N., Jiang, W., 2018. In vitro and in vivo DFO-chelatable labile iron release profiles among commercially available intravenous iron nanoparticle formulations. *Regulatory Toxicology and Pharmacology*. 97, 17–23. <https://doi.org/10.1016/j.yrtph.2018.05.014>
- Pharmacopoeia B. Iron Sucrose Injection British Pharmacopoeia.
- Qi, S.F., Zhang, J., Wang, Y., Ning, S., 2011. Determination of total iron in iron ore by potentiometric titration with ascorbic acid as reducing titrant. *Rock & Mineral Analysis*. 31, 63–66.
- Shah, R.B., Yang, Y., Khan, M.A., Raw, A., Yu, L.X., Faustino, P.J., 2014. Pharmaceutical characterization and thermodynamic stability assessment of a colloidal iron drug product: Iron sucrose. *International Journal of Pharmaceutics*. 464(1–2), 46–52. <https://doi.org/10.1016/j.ijpharm.2014.01.008>
- Silverstein, S.B., Rodgers, G.M., 2004. Parenteral iron therapy options. *American Journal of Hematology*. 76(1), 74–8. <https://doi.org/10.1002/ajh.20056>
- Sun, D., Rouse, R., Patel, V., Wu, Y., Zheng, J., Karmakar, A., Patri, A.K., Chitranshi, P., Keire, D., Ma, J., Jiang, W., 2018. Comparative evaluation of U.S. brand and generic intravenous sodium ferric gluconate complex in sucrose injection: Physicochemical characterization. *Nanomaterials*. 8(1). <https://doi.org/10.3390/nano8010025>
- Swift, E.H., 1929. The iodometric determination of iron. *Journal of the American Chemical Society*. 51(9), 2682–2689. <https://doi.org/10.1021/ja01384a011>
- Tabasi, O., Razlighi, M.R., Darbandi, M.A., 2021. An optimized process for the preparation of aqueous ferric carboxymaltose: Synthesis and structural characterization. *Pharmaceutical Nanotechnology*. 9(2), 157–163. <https://doi.org/10.2174/2211738509666210114160941>
- Tesoro, A., Novakovic, J., Thiessen, J.J., Spino, M., 2005. Validated HPLC assay for iron determination in biological matrices based on ferrioxamine formation. *Journal of Chromatography B: Analytical Technologies in the Biomedical and Life Sciences*. 823(2), 177–183. <https://doi.org/10.1016/j.jchromb.2005.06.033>
- Using DLS, ELS and SAXS to Study Ferric Nanoparticles Stabilized Using Different Oligosaccharides. Anton Paar application note.
- Venofer® (Iron Sucrose Injection) Labeling.
- Wu, Y., Petrochenko, P., Chen, L., Wong, S.Y., Absar, M., Choi, S., Zheng, J., 2016. Core size determination and structural characterization of intravenous iron complexes by cryogenic transmission electron microscopy. *International Journal of Pharmaceutics*. 505(1–2), 167–174. <https://doi.org/10.1016/j.ijpharm.2016.03.029>
- Zou, P., Tyner, K., Raw, A., Lee, S., 2017. Physicochemical characterization of iron carbohydrate colloid drug products. *American Association of Pharmaceutical Scientists*. 19(5), 1359–1376. <https://doi.org/10.1208/s12248-017-0126-0>
2010. Parenteral irons: Indications and comparison. *U.S. Pharmacist*. 35(11), HS-22–HS-24.